Received: 21 January 2023 | Revised: 23 June 2023 | Accepted: 28 June 2023

DOI: 10.1002/mrc.5379

WILEY

SPECIAL ISSUE RESEARCH ARTICLE

Contributions towards variable temperature shielding for compact NMR instruments

Martin Bornemann-Pfeiffer[1,2] | **Klas Meyer**[1] | **Jeremy Lademann**[1] | **Matthias Kraume**[2] | **Michael Maiwald**[1]

[1]Bundesanstalt für Materialforschung und -prüfung, Berlin, Germany

[2]Chair of Chemical and Process Engineering, Technical University Berlin, Berlin, Germany

Correspondence
Michael Maiwald, Bundesanstalt für Materialforschung und -prüfung (BAM), Richard-Willstätter-Straße 11, Berlin 12489, Germany.
Email: michael.maiwald@bam.de

Abstract

The application of compact NMR instruments to hot flowing samples or exothermically reacting mixtures is limited by the temperature sensitivity of permanent magnets. Typically, such temperature effects directly influence the achievable magnetic field homogeneity and hence measurement quality. The internal-temperature control loop of the magnet and instruments is not designed for such temperature compensation. Passive insulation is restricted by the small dimensions within the magnet borehole. Here, we present a design approach for active heat shielding with the aim of variable temperature control of NMR samples for benchtop NMR instruments using a compressed airstream which is variable in flow and temperature. Based on the system identification and surface temperature measurements through thermography, a model predictive control was set up to minimise any disturbance effect on the permanent magnet from the probe or sample temperature. This methodology will facilitate the application of variable-temperature shielding and, therefore, extend the application of compact NMR instruments to flowing sample temperatures that differ from the magnet temperature.

KEYWORDS

benchtop NMR, continuous processes, inline analytics, model predictive control, process analytical technology, temperature control

1 | INTRODUCTION

Compact NMR instruments have extensive applications,[1–3] including reaction and process monitoring.[4–7] Unlike high-field NMR, compact NMR instruments are not restricted to laboratory applications because process analytical technology analysers based on these instruments have been demonstrated at industrial scales.[8,9] The availability of rare-earth permanent magnetic materials in combination with magnet array designs[10] was an important foundation for the development of compact NMR instruments with acceptable weight and sufficient field strength and homogeneity[11] without the need for cryogens.

A disadvantage of using permanent magnets is the dependence of the magnetic field strength and field homogeneity on even the smallest changes in magnet temperature.[12–14] As shown in Figure 1, magnet

temperature deviations of less than $\Delta T = 0.01$ K can result in distorted NMR spectra. Relatively slow changes or negligible deviations in the magnet temperature occurring as a consequence of daily fluctuations in room temperature or insertion of NMR tube samples with varying temperatures can be compensated for by using an internal temperature control loop. The precise implementation of this control loop is the proprietary design of each manufacturer. To the best of our knowledge, these systems comprise multiple temperature sensors and corresponding Peltier elements for active temperature control of the magnet, electronic components, and instrument housing. For standard applications, such as sample analysis in NMR tubes, and most flow applications around room temperature, the internal controller can appropriately maintain a stable operation of the magnet without severe, temperature-induced fluctuations in magnetic field homogeneity. When 5 mm NMR tubes are placed in the magnet, the amount of heat transferred between the NMR magnet and the NMR sample tube at room temperature is sufficiently small. Slight deviations from the magnet temperature in flowing samples can be tolerated when flow-through cells are used. However, when studying chemical reactions or monitoring processes, it may be necessary for the reaction to take place in the NMR instrument itself, or the sample stream may need to be maintained at a temperature much higher or lower than the magnet temperature.[15] In such cases, the heat flux between sample volume and NMR magnet is rapidly increasing and may no longer be compensated by the internal temperature control loop as shown in Figure 1 carrying out a continuous chemical acetylation reaction: Because the magnet temperature increases with the liquid sample temperature, (i) the internal variables of the instrument (*Power*1 and *Power*2) controlling the magnet temperature decrease (Figure 1b, blue symbols), leading to a decreasing magnet temperature (Figure 1a, black curve) at first. As the manipulated variables reach their lower boundary (at ∼20 min), the magnet temperature rises again until the chemical reaction is stopped (Figure 1a at ∼28 min, red curve). The highest magnet temperature (ii) is reached shortly afterwards with a delay. This effect can be tolerated for a short time but has deteriorating effects on magnetic field homogeneity, as demonstrated in Figure 1c.

A heat source within an NMR magnet is by far not new. Measurements at varying probe temperatures are commonly performed in high-field NMR experiments; commercial and custom-made variable-temperature probes are available for this purpose.[16–18] These probes adjust the sample temperature through either an electric heater in combination with air or gaseous nitrogen flow or a fluorinated liquid. Despite the nonnegligible heat

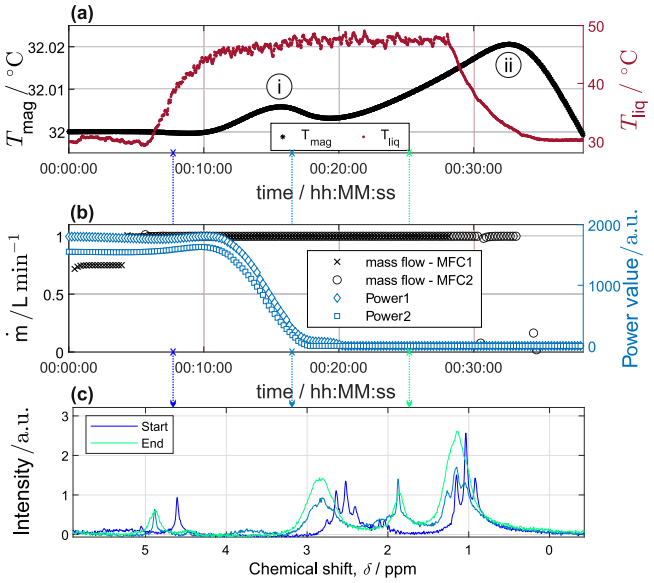

FIGURE 1 Continuous chemical acetylation within the NMR magnet demonstrating overheating: (a) course of the reaction mixture temperature and corresponding NMR magnet temperature, with coloured indication of the time the spectra was acquired (vertical arrows from a to c) and local maxima of the magnet temperature (i/ii). (b) Mass flow of the reactant benzyl alcohol with triethylamine and acetyl chloride and two internal power control variables of the NMR instrument (*Power*1 and *Power*2 are arbitrary internal control variables driving the actuators). (c) Superimposed spectra with an indication of the time of measurement, which deteriorate with time.

flux between the thermostated sample and the magnet, the homogeneity of the magnetic field is less impaired compared with the case of permanent magnets in compact NMR instruments, as the magnetic field homogeneity of the electromagnet is less sensitive to temperature changes.

The inline analysis of exothermic reaction mixtures or mixtures with a significantly higher temperature than that of the NMR magnet is a particular case of application. To the best of our knowledge, none of the compact NMR instrument manufacturers proved a commercially available integral active temperature control or sufficient probe temperature shielding and insulation for a longer experiment or continuous operation at a deviating sample temperature. Some of the available instruments can heat up the whole magnet. Still, they focus on maintaining a constant probe temperature within a sample tube for offline applications (e.g., for mimicking fixed reaction conditions). However, reshimming the instrument after changing the magnet temperature is time-consuming and cumbersome, as shim sets vary widely from each other. Current publications have addressed the issue of temperature effects of NMR measurement quality[2,13,19] without

providing potential solutions for active shielding or passive insulation.

As discussed later, developing an efficient temperature control is impeded by two boundary conditions. First, the internal instrument control loop works independently of a newly developed temperature control system. To avoid the mutual interference of both control loops, fluctuation in the heat flux from the flowing sample to the NMR magnet must be reduced. Second, comprehensive access to relevant temperature sensing (e.g., surface temperatures within the instrument or the probe) can only be achieved with major hardware modifications. Therefore, a substitute system (introduced in Section 3.1) is developed in this study, which allows access to the surface temperature and later application to different instruments. Based on surface temperature sensing, a controller for active temperature control is developed (Section 3.2) and successfully validated (Section 3.3).

2 | CONCEPT AND STRATEGY

The aim of this work is to contribute to the thermal decoupling of the sample feedthrough from the permanent magnet of a benchtop NMR spectrometer. Preliminary investigations with passive insulation did not prove to be effective enough, although there was access to state-of-the-art materials, such as modified fumed silica (aerosil[20]).

Thankfully, we had a wide bore compact NMR prototype with a 12 mm inner diameter at our disposal (Nanalysis Corp., Calgary, Alberta, Canada), which conceptually can also serve as a basis for typical sample port designs. Initially, a double-flow design was adopted, with one airstream regulating the NMR sample temperature and the other airstream thermally separating the sample from the surrounding NMR magnet. However, this design is complex due to its many filigree concentric tubes and low wall strengths. As a result, the preliminary experiments could not achieve effective sample temperature control and simultaneous thermal decoupling of the NMR magnet. Hence, the control target is solely the thermal decoupling of the NMR magnet.

2.1 | Variables affecting measurement quality

The magnet used in compact NMR instruments is an array of small and, in most cases, prismatic, rare-earth permanent magnets. The arrangement proposed by Halbach[10] remains superior and is used by most manufacturers. The available energy difference in the various nuclei states and, hence, the achievable signal sensitivity depends linearly on the magnetic flux density of the instrument. Increasing the field strength by a compact design limits the free space available around the sample head. The overall magnetic field homogeneity achievable at the measurement volume depends on the structure of the Halbach array (e.g., number and position of the single magnets and length-to-radius ratio of the magnet array[21]), as well as the perturbations of the single magnets themselves.[22] Existing inhomogeneities of the magnetic field can be overcome by adjusting the position of movable permanent magnet blocks and the current of auxiliary electric coils, known as shim coils, during a shim procedure.[11] Another important factor is the filling factor, defined as the volume of the liquid sample within the receiver coil divided by the overall volume of the receiver coil. A filling factor close to its maximum value results in a high signal-to-noise ratio, which can be further improved using optimised coil volumes (e.g., micro coils[23,24] or an inner inductively coupled coil[25]). A good filling factor also limits the available space in the immediate vicinity of the sample cell, for example, for temperature insulation.

2.2 | Temperature shielding strategies

Strategies to minimise the heat flux between sample probe and magnet are generally distinguished as passive (hereinafter, insulation) or active (hereinafter, temperature shielding). The first choice of insulation is a Dewar, which is a typical silver-mirrored double-walled vessel containing a vacuum and was discarded due to the absorption of radio frequency of the coating. A Dewar without mirror coating containing polytetrafluoroethylene (PTFE) tubing was tested but did not prove sufficient insulation leading to an intolerable increase of magnet temperature (results are shown in Figure S2). Another approach is to minimise heat conduction by introducing a separation with low thermal conductivity. Thermal resistance increases with insulation layer thickness, usually resulting in thick layers. As mentioned earlier, this approach is limited because of the low filling factor (sensitivity). A larger borehole in the magnet leads to an exponentially increasing requirement in the magnet design to obtain the same field strength.[26] In addition, classical insulation only reduces the heat flux and slows down the temperature compensation process. In the case of long-lasting heat input, the magnet heats up as well (see Figure S2). The shielding strategies examined in this study are shown in Figure 2.

In contrast, a more suitable choice of temperature shielding using a fluid (hereinafter, $Fluid_{iso}$) to dissipate the heat flux was developed. Controlled mass flow and temperature of the $Fluid_{iso}$ enable a flexible drain of energy to compensate for constant and even periodically occurring heat of reaction. A usual choice of the $Fluid_{iso}$ is a liquid cooling agent, such as (tri)ethylene glycol, ethanol, or water. However, in our case, the choice is limited, as the $Fluid_{iso}$ flows within the NMR coil (Figure 3); hence, any protonated liquid cooling agent would be observed on the measured NMR spectra. An alternative is the use of liquid perfluorinated hydrocarbons (e.g., perfluoro decalin or perfluoro tributylamine), as they do not interfere with the actual ^{1}H spectra acquisition[17] but are discarded due to their persistent environmental impact and greenhouse potential. Therefore, pressurised air was selected as a cheap and available alternative in this study. Its low heat capacity compared with that of liquid agents was not a severe drawback, as the overall thermal energy which needs to be dissipated was quite small (e.g., $Q_{loss} = 3.84$ W) for the previously shown experiment (Figure 1 and Supporting Information S1, Preliminary Studies).

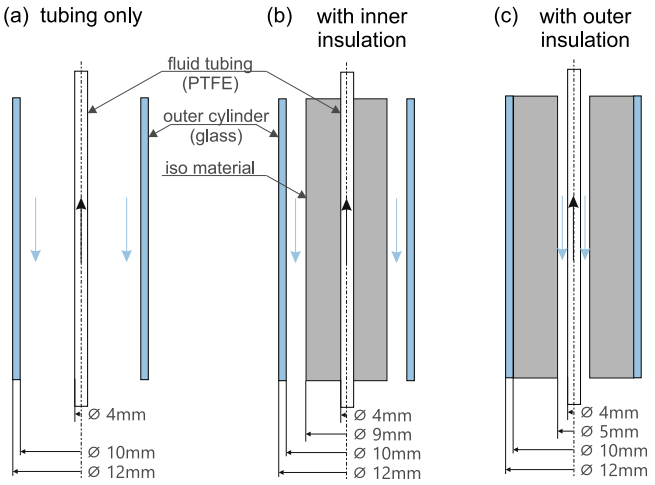

FIGURE 2 Simplified insulation/temperature shielding concepts for a potential 4 mm fluid tubing carrying the reaction mixture: (a) temperature shielding only and no additional passive insulation; (b) temperature shielding and additional 'inner' insulation; and (c) temperature shielding and additional 'outer' insulation.

A potential controller uses the flow and temperature of the $Fluid_{iso}$ as manipulated variables to fulfil its regulatory objectives. The main objective is to maintain a constant magnet temperature, which is already the objective of the internal instrument control loop. As mentioned in Section 1, this internal control loop is designed to cope with slow deviations in the magnet temperature (e.g., daily fluctuations in the laboratory room temperature) using actuators like Peltier elements for subsequent cooling or heating. We have therefore based our control concept on shielding all temperature fluctuations within the sample cell as far as possible from the area of the magnet. As the conducted experiments have shown, the main danger is to disturb the sensitive magnetic control circuit of the device, provoking protracted thermoregulation activities accompanied by temporary changes in magnetic field homogeneity. Access to the control parameters of the device and magnet temperature control is currently not provided by any manufacturer for confidentiality reasons.

Therefore, the main objective of the proposed approach is to reduce fluctuation in the heat flux from the probe to the magnet to minimise the influence of the

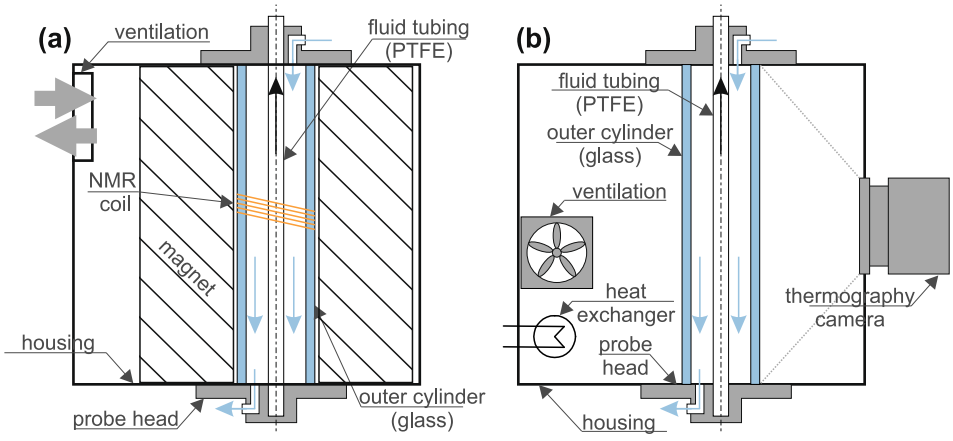

FIGURE 3 (a) Physical set-up within the NMR instrument. Two concentric pipes within the magnet borehole: outer glass cylinder as the separation between the insulation flow stream and instrument. Inner PTFE tubing containing the liquid fluid to be measured. Connection flanges on top and bottom containing the fluid connectors are custom made of polyoxymethylene. (b) NMR substitute box with thermography camera and temperature control unit.

internal control loop on the reaction mixture. The heat flux itself is, in general, not directly measured but is accessible through the relevant temperature difference in this case (between the magnet [T_{mag}] and the adjacent glass capillary surface holding the measurement coil [T_{sur}]).

3 | RESULTS AND DISCUSSION

3.1 | Design of the experimental set-up

In an NMR instrument, the surface temperature cannot be accessed entirely. Therefore, an NMR substitute box (see Figure 3b for the simplified scheme) was designed to mimic the conditions in an NMR instrument and access the temperature control set-up through optical thermography. The optical thermography enables the measurement of the surface temperature T_{sur} at a sufficiently high measurement rate (0.5 s^{-1}) and a resolution of 0.4 mm^2 per pixel. Further information on the thermography can be found within Supporting Information S1, Thermographic Measurements. In the simplest case, variable-temperature shielding comprises two concentric pipes. While the inner tube contains the sample fluid, which is to be measured, the annulus contains the insulation fluid (in our case, pressurised air), which is required to remove heat energy from the system. Additional passive insulation, as shown in Figure 2b,c, was examined in the preliminary studies (results are shown in Supporting Information S1, Passive Insulation) and discarded as it could not significantly reduce T_{sur}. The additional passive insulation connected to the outer cylinder (Figure 2c) introduced an additional delay time for the control system, impeding the control task. In contrast, additional passive insulation connected to the fluid tubing helps improve the overall shielding performance but was not necessary for the examined reaction (Figure 2b).

The substitute box was later replaced with the actual wide bore NMR prototype instrument (Figure 3a), but the surrounding piping and instrumentation (Figure 4) remained the same. Changes occurred in the surface temperature measurement (replacement of the IR thermography camera with thin-film thermocouples and that of the substitute box with the NMR instrument). More details and photographs of the set-up are shown in Figures S5–S10.

3.2 | Temperature control model

The dependency of T_{sur} on the substitute box temperature T_{box} and the ingoing and outgoing fluid streams can be derived from the energy balances of the set-up. Although the underlying physics of heat transfer within a system of concentric pipes or tubes are well understood, deviations between the model and physical reality are unavoidable. Several methods available can help improve the model fit (e.g., simplifying the models through parameter lumping, parameter fixing or parameter omitting,[27] and using empirical correction terms). As the model will be later used for synthesising the controller and would need further transformation and improvement, first principle models are discarded here and replaced with an empirical, state-space model (see Equations 1 and 2) providing a better fit to the experimental data.

According to Ljung,[28] the model development or system identification involves two steps: first, the choice of a

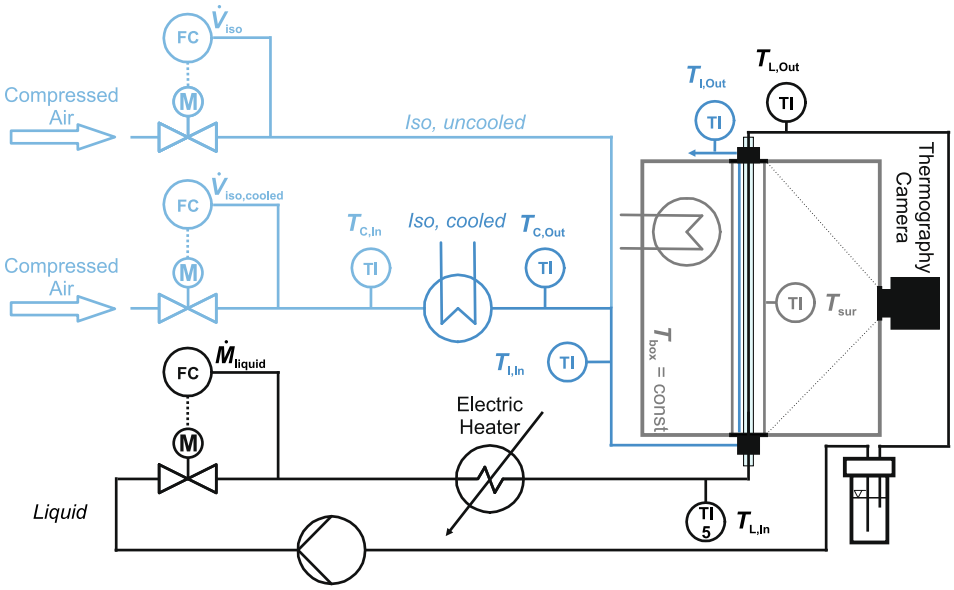

FIGURE 4 Scheme of the temperature-regulated NMR substitute box containing the box temperature control unit (ventilation and heat exchanger), probe piping with mass flow controller and pump and thermography device.

mathematical model of the smallest dimension, which is described by a set of parameters, and second, identification of these parameters through the experimental data by a fitting routine. A widely spread model structure is the so-called state-space form related to the system input(s), u^*, and output(s), y, through first-order differential equations (indicated by a dot above the variable) using auxiliary state variable(s), x.

$$\dot{x} = Ax + Bu^* \text{ with } \quad u^* = \begin{pmatrix} u \\ z \end{pmatrix}, \tag{1}$$

$$y = Cx + Du. \tag{2}$$

Here, A, B, C, and D are—depending on the number of states, inputs, and outputs—variables, vectors, or matrices. Due to their determined structure, on the one hand, and the flexible number of states, x, on the other hand, state-space representations are well suited to model the dynamic behaviour of many systems with single or multiple inputs and outputs. This approach is widely used in control engineering, and many controller synthesis procedures are based on state-space forms. For simplicity, we adopt a linear time-invariant structure which produces a sufficient model match in many cases. The model parameters are identified by minimising of the prediction error using the measured data and a numerical optimisation routine.[29]

The system output T_{sur} is physically dependent on many other dynamic variables. Therefore, a model structure involving multiple inputs and a single output variable is chosen. The input variables u^* are further divided (Table 1) into manipulated variables u, which are the actuators of the controller, and the measured disturbances z considered within the model. A meaningful choice of the considered measured disturbances is achieved by performing a sensitivity analysis using the minimum redundancy maximum relevance algorithm,[30] discarding the less relevant inputs.

To achieve a high similarity between the computational model and physical system, meaningful and, therefore, representative data are required. If applicable, as in the given case, a design of experiment, including all manipulable system inputs, will yield the best results. Following standard textbooks, inputs should be perturbed simultaneously and uncorrelated.[28,31] Commonly used inputs are pseudo-random binary or multisinusoidal[32] sequences. In this study, a combination of multisinusoidal inputs and the course of the manipulated variables based on the controller decisions of an earlier experimental run (Figure 5, yellow dashed boxes) yielded the best results. During single excitation periods, the uncorrelated response of the system output to the single system inputs was examined, while the common excitation period revealed potential cross-correlations. The additional system input from the earlier experimental run revealed system dynamics under actual operation conditions.

The influence of single disturbances and manipulated variables (especially cooled insulation flow and fluid temperature) on the surface temperature T_{sur} can be clearly seen throughout the experimental identification run. The state-space model was estimated through state-of-the-art

TABLE 1 Variable allocation of the finally identified model containing control variables, manipulated variables, and measured disturbances.

Variable name	Unit	Short	Allocation	
T_{sur}	°C	y (1)	Control variable	y
$\dot{V}_{iso}$	L min^{-1}	u (1)	Manipulated variable	u
$\dot{V}_{iso,cooled}$	L min^{-1}	u (2)	Manipulated variable	u
$\dot{M}_{liquid}$	g min^{-1}	z (1)	Measured disturbance	z
T_{liq}	°C	z (2)	Measured disturbance	z
T_{box}/T_{mag}	°C	z (3)	Measured disturbance	z
$T_{I,in}$	°C	z (4)	Measured disturbance	z
$T_{I,out}$	°C	z (5)	Measured disturbance	z
$T_{C,in}$	°C	z (6)	Measured disturbance	z
$T_{C,out}$	°C	z (7)	Measured disturbance	z
*Power*1	a. u.	z (8)	Measured disturbance	z
*Power*2	a. u.	z (9)	Measured disturbance	z

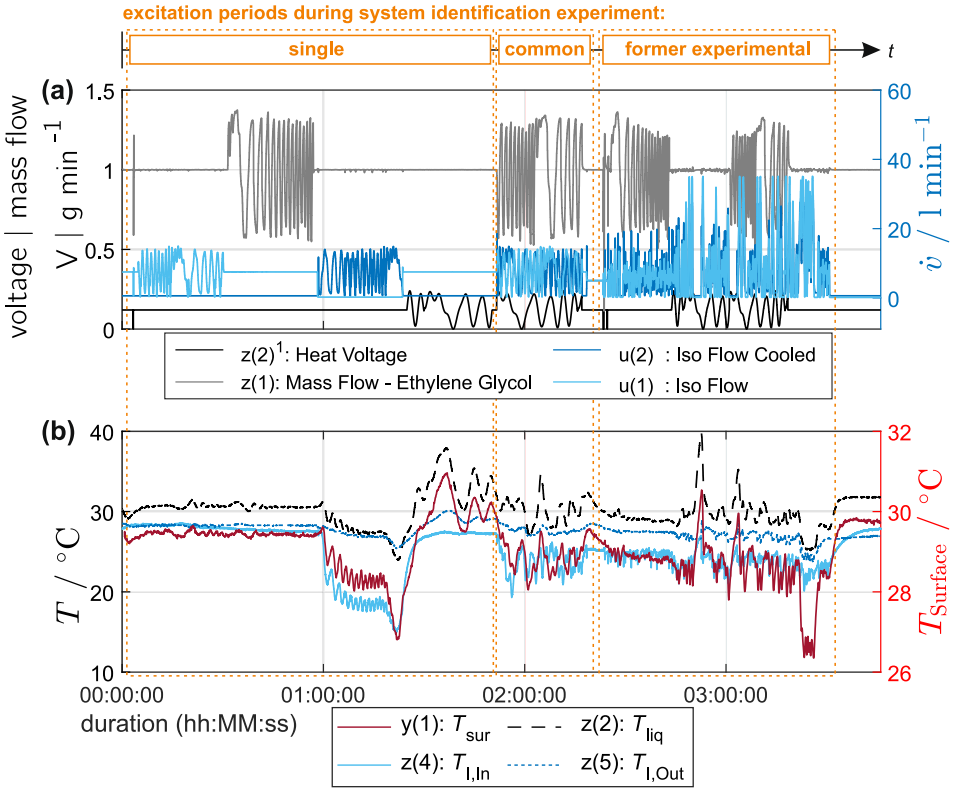

FIGURE 5 System identification experiment consisting of (a) single multisinusoidal excitations of model inputs with one common excitation period, followed by a former experimental run with a controller. (b) Development of relevant temperatures within the system.[1] Heating wire voltage as an auxiliary variable raising the liquid temperature T_{liq}.

numerical prediction error minimisation. Additional details can be found in Supporting Information S1, Controller.

There are many potential types of controllers for multiple input single output systems (e.g., linear–quadratic–Gaussian, H-infinity, and model predictive control [MPC]).[33] Here, a linear MPC approach was selected, as many disturbance variables are accessible through direct measurement and hence can be considered in the future controller action calculation. An MPC solves a quadratic programming optimisation problem within each control interval, considering a cost function and given constraints. The standard cost function consists of several terms with individual weights, allowing for a specific controller tuning. The following terms were part of the cost function: control variable reference tracking, manipulated variable tracking, manipulated variable movement suppression, and constraint violation. The tuning of the controller is, despite available performance measures[34] and tuning guidelines,[35] an iterative process. The finally applied parameter can be found in Table S2.

3.3 | Results

For the demonstration of the positive effect of temperature control, three experiments each were performed on the NMR substitute box and the real NMR wide bore prototype: (a) no insulation air stream at all, (b) constant insulation air stream, and (c) fully MPC controlled insulation air stream. Experiments with the NMR substitute box are described only in Supporting Information S1 for clarity (see Figures S11 and S12).

After successfully evaluating the variable-temperature shielding within the NMR substitute box through optical thermography, the set-up was retransferred into the compact NMR wide bore prototype instrument for validation purposes. During experimentation within the NMR substitute box, no significant geometric surface temperature gradient was revealed; hence, the IR camera was replaced with three equally distanced thin-film thermocouples. The average temperature value now representing T_{sur}. It should be noted again that the available compact wide bore NMR device with 60 MHz proton frequency is a prototype device with an increased coil diameter of 12 mm. This device was modified by Nanalysis for our specific application. Consequently, due to the reduced filling factor, the achievable linewidths are by no means comparable with products or solutions available on the market. The aim of this project was solely to create a suitable design basis that can be adapted to specific applications and not to demonstrate the highest achievable line widths.

The following experimental runs were conducted with the NMR substitute box (see Supporting

Information S1, NMR Substitute Box Results) and within the NMR wide bore prototype (shown below):

$$\text{(a) constant insulation air stream}, u = \begin{pmatrix} \text{const.} \\ \text{const.} \end{pmatrix},$$

$$\text{(b) MPC controlled insulation air stream}, u = \begin{pmatrix} f(w,y,z \\ f(w,y,z \end{pmatrix},$$

$$\text{(c) no insulation air stream at all}, u = \begin{pmatrix} 0 \\ 0 \end{pmatrix}.$$

The results of variants (a) and (b) are shown in Figure 6. Further information as well as the results of variant (c) can be found in Figures S17 and S18. During the uncontrolled run (a), the course of the magnet temperature as well as the internal temperature control variables ($z(8)$ and $z(9)$) of the instrument is strongly fluctuating, leading to a maximum deviation of the magnet temperature, max $(\Delta T_{\text{mag}}) = \pm 0.01$ K. Furthermore, it can be seen that the internal control variable $z(8)$ is reaching its minimal restriction during experimentation indicating the limit of temperature compensation of the compact NMR instrument. The effect on the recorded spectra is clearly visible through the change of the peak shapes and line widths during the experiment (Figure 6a, bottom). These changes even prevent characterisation of the spectra quality through full width at half maximum measurement over the full period of the experimentation because the two signals of the NMR spectrum merge.

In comparison with that, the MPC controlled run (Figure 6b) results into a by factor 7:1 reduced magnet temperature fluctuation of max $(\Delta T_{\text{mag}}) = \pm 0.0014$ K while ensuring an almost steady course of $z(8)$ and $z(9)$. As can be seen in the acquired spectra (Figure 6b, bottom), the shape and signal line widths remain almost constant, a prerequisite for, for example, evaluation of overlapping substance peaks. The internal control variables not only indicate an existing potential for even higher fluid temperatures but also remain almost constant under changing temperature loads. Hence, a stable

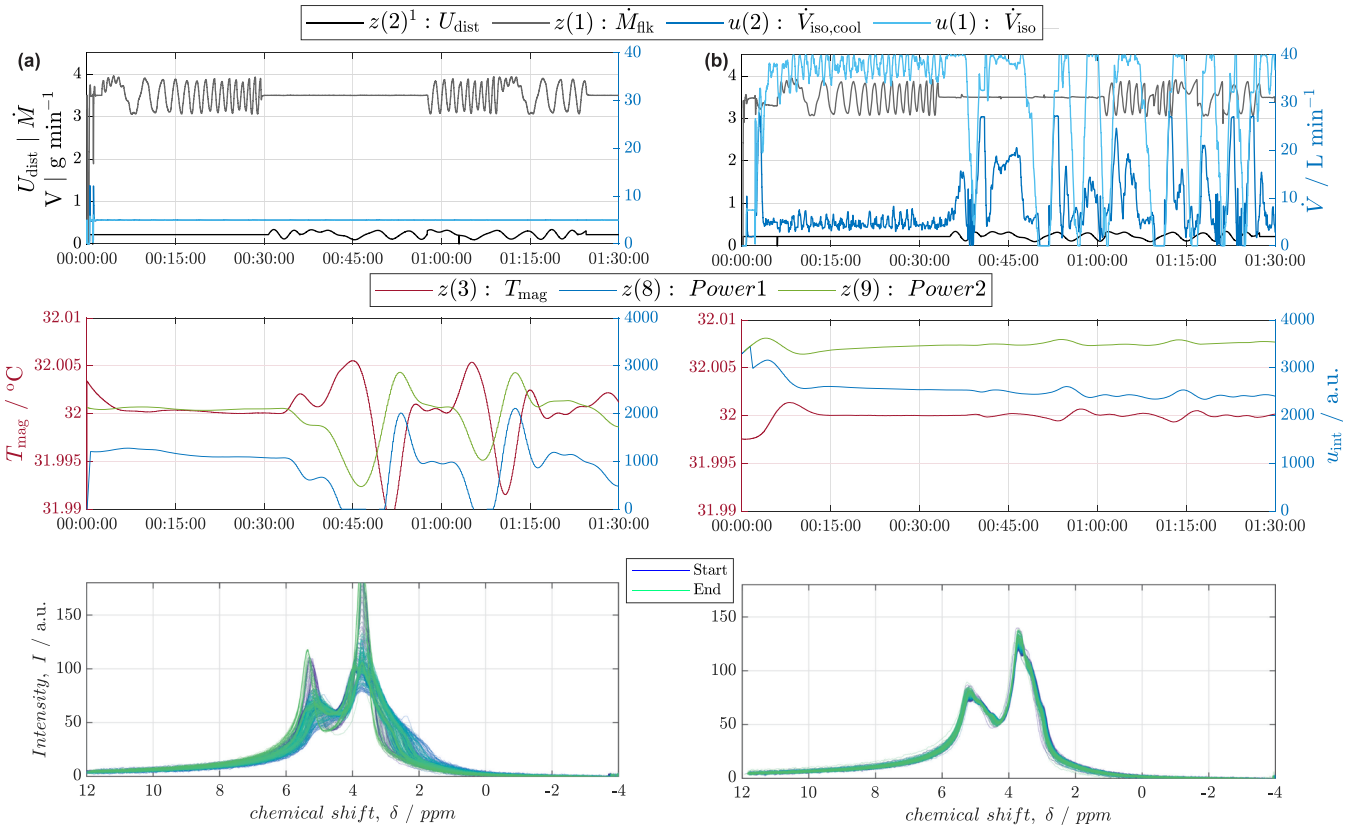

FIGURE 6 Two experimental runs within the compact NMR wide bore prototype instrument distinguishable as variants: (a) 'Constant Iso Flow', that is, steady isolation insulation flow, and (b) 'MPC', that is, MPC controlled ($w = 0$). Opposed in each case are as follows: (top) The course of the disturbance variables $z(1)$ and $z(2)$ as well as manipulated variables $u(1)$ and $u(2)$. Both manipulated variables are set up with an upper limit of 40 L min^{-1}. (middle) Course of the NMR magnet temperature, $z(3)$, and temperature control parameters of the instrument, $z(8)$ and $z(9)$. (bottom) Plot of the stacked spectra during experimentation which were recorded with. Legends apply for both horizontal panels.

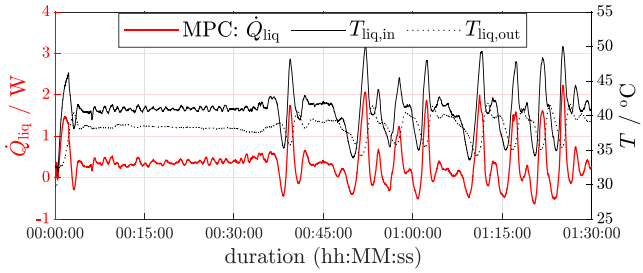

FIGURE 7 Model predictive control (MPC) controlled experimental run (same as shown in Figure 6b) within the compact NMR wide bore prototype instrument: calculated heat introduced into the system by the liquid probe and corresponding temperatures. The negative heat flow is caused by the lower mass flow of the liquid probe compared with the insulation air flow.

magnetic field homogeneity for consistent spectra quality could be ensured.

$$\dot{Q}_{liq} = \dot{m}_{liq} \cdot c_{P,liq} \cdot \left(T_{liq,in} - T_{liq,out}\right). \quad (3)$$

The thermal energy introduced by the sample was determined according to the simplified energy balance (Equation 3), assuming quasi-steady-state and isobaric conditions. During the relevant MPC controlled run (Figure 6), an average amount of 0.4 W thermal energy was introduced over the course of the experiment (Figure 7). Much more meaningful, however, is the consideration of the maximum heat flow $Q_{max} = 2.2$ W and the largest rate of change of approximately $dT/dt = 0.05$ K s^{-1} which is the critical parameter as shown in the prior results. However, due to the different characteristics of set-ups and compact NMR instrument, these parameters can only serve as a guide value for other set-ups.

4 | CONCLUSION

In this study, a controlled variable-temperature shielding set-up was realised, which applies to compact NMR instruments. A heat load of up to 2.2 W, in this particular case, was counterbalanced using thermostated air flows without additional insulation. For confidentiality reasons, the controller was set up independently of the NMR internal magnet temperature control system. Although this is not as desirable as a holistic approach, it allows for easy transferability to other instruments. To gain access to the surface temperature of the outer glass tube, by separating the borehole from the magnet, the set-up was transferred to an NMR substitute box for preliminary experiments allowing easier access to surface temperatures.

Two major findings were obtained from this study. First, additional passive insulation was not beneficial, as it decelerated the internal system dynamics and thus impeded the overall controllability of the test case studied. Second, the combination of two different manipulated variables (insulation air flows of different temperature) showed an excellent controller performance regarding rapid changes in thermal load. Additionally, the set-up was reinserted into the NMR instrument as a proof of concept. The experimental findings suggested an efficient temperature shielding. The minimisation of interference between the inner instrument and external temperature shielding control loop was crucial for the successful implementation within the instrument.

It should be noted that the space requirement for the presented variable-temperature shielding competes with the demand for low fill factors and thus small spectral linewidths. Commercially available instruments are not compatible with the presented method without prior hardware modifications, as they come standard with 5 mm coils aimed at the highest spectral resolution without adequate control of the thermal stress that occurs in exothermic continuous chemical reactions. The ability to modify NMR instruments for larger coil diameters is generally available on all instruments. However, a holistic control approach that incorporates the temperature control loops internal to the instrument and a substantial improvement in spectrum quality will require the cooperation of the manufacturers in all cases. We hope that this paper will provide a solid basis for future design guidelines.

ACKNOWLEDGEMENTS

First and foremost, we would like to thank Nanalysis Corp., Calgary, Alberta, Canada, for providing the wide bore NMR prototype and valuable assistance in using this instrument. In particular, the support of Juan Araneda and Neal Gallagher for discussion and support as well as Martin Berberov and Greg McFeetors for their help regarding out-of-spec magnet shimming (all Nanalysis Corp., Calgary, Alberta, Canada) is gratefully acknowledged. Furthermore, we thank Simon Kern (S-Pact GmbH) for the discussion and initial ideas. We thank Christoph Naese (BAM) for his fast and reliable support in designing and building customised construction parts. We thank our colleagues from the BAM Division 8.7 "Thermographic Methods" for their support. Finally, we acknowledge the support from Björn Hagedorn and Parastoo Semnani, whose experimental work in preliminary studies produced the first foundation to build this work.

CONFLICT OF INTEREST STATEMENT

The authors would like to mention that the wide bore prototype was acquired on a paid loan basis from Nanalysis Corp. of Calgary, Alberta, Canada, for most of the experimental work presented here.

PEER REVIEW

The peer review history for this article is available at https://www.webofscience.com/api/gateway/wos/peer-review/10.1002/mrc.5379.

ORCID

Martin Bornemann-Pfeiffer https://orcid.org/0000-0003-1758-4594

REFERENCES

[1] M. Grootveld, B. Percival, M. Gibson, Y. Osman, M. Edgar, M. Molinari, M. L. Mather, F. Casanova, P. B. Wilson, *Anal. Chim. Acta* **2019**, *1067*, 11.
[2] T. A. van Beek, *Phytochem. Anal.* **2021**, *32*, 24.
[3] T. Castaing-Cordier, D. Bouillaud, J. Farjon, P. Giraudeau, in *Annual Reports on NMR Spectroscopy*, (Ed: G. A. Webb) Vol. 103, Academic Press, Burlington House, Piccadilly, London, United Kingdom **2021**, 191.
[4] F. Dalitz, M. Cudaj, M. Maiwald, G. Guthausen, *Prog. Nucl. Magn. Reson. Spectrosc.* **2012**, *60*, 52.
[5] A. Friebel, E. von Harbou, K. Münnemann, H. Hasse, *Ind. Eng. Chem. Res.* **2019**, *58*, 18125.
[6] K. Meyer, S. Kern, N. Zientek, G. Guthausen, M. Maiwald, *TrAC, Trends Anal. Chem.* **2016**, *83*, 39.
[7] J. Giberson, J. Scicluna, N. Legge, J. Longstaffe, in *Annual Reports on NMR Spectroscopy*, (Ed: G. A. Webb) Vol. 102, Academic Press, Burlington House, Piccadilly, London, United Kingdom **2021**, 153.
[8] S. Kern, L. Wander, K. Meyer, S. Guhl, A. R. G. Mukkula, M. Holtkamp, M. Salge, C. Fleischer, N. Weber, R. King, S. Engell, A. Paul, M. P. Remelhe, M. Maiwald, *Anal. Bioanal. Chem.* **2019**, *411*, 3037.
[9] W. G. Lee, M. T. Zell, T. Ouchi, M. J. Milton, *Magn. Reson. Chem.* **2020**, *58*, 1193.
[10] K. Halbach, *Nuclear Instruments and Methods* **1980**, *169*, 1.
[11] E. Danieli, J. Mauler, J. Perlo, B. Blümich, F. Casanova, *J. Magn. Reson.* **2009**, *198*, 80.
[12] N. Zientek, K. Meyer, S. Kern, M. Maiwald, *Chem. Ing. Tech.* **2016**, *88*, 698.
[13] N. Nestle, Z. J. Lim, T. Böhringer, S. Abtmeyer, S. Arenz, F. C. Leinweber, T. Weiß, E. von Harbou, *Magn. Reson. Chem.* **2020**, *58*, 1213.
[14] K. Meyer, J. Ruiken, M. Illner, A. Paul, D. Müller, E. Esche, G. Wozny, M. Maiwald, *Meas. Sci. Technol.* **2017**, *28*, 035501.
[15] M. Bornemann, S. Kern, N. Jurtz, T. Thiede, M. Kraume, M. Maiwald, *Ind. Eng. Chem. Res.* **2019**, *58*, 19562.
[16] A. M. R. Hall, T. A. A. Cartlidge, G. Pileio, *J. Magn. Reson.* **2020**, *317*, 106778.
[17] A. Brächer, S. Hoch, K. Albert, H. J. Kost, B. Werner, E. von Harbou, H. Hasse, *J. Magn. Reson.* **2014**, *242*, 155.
[18] B. Wouters, P. Miggiels, R. Bezemer, E. A. W. van der Cruijsen, E. van Leeuwen, J. Gauvin, K. Houben, K. B. S. S. Gupta, P. Zuijdwijk, A. Harms, A. C. de Souza, T. Hankemeier, *Anal. Chem.* **2022**, *94*, 15350.
[19] M. V. Silva Elipe, R. R. Milburn, *Magn. Reson. Chem.* **2016**, *54*, 437.
[20] Evonik Industries AG, (n.d), *The Chemical All-Rounder the Fumed Silica AEROSIL*, https://history.evonik.com/en/inventions/aerosil, accessed December 30, 2022.
[21] S. Tewari, T. O'Reilly, A. Webb, *J. Magn. Reson.* **2021**, *324*, 106923.
[22] K. Halbach, *Nuclear Instruments and Methods in Physics Research* **1982**, *198*, 213.
[23] R. M. Fratila, A. H. Velders, *Annual Review of Analytical Chemistry* **2011**, *4*, 227.
[24] S. S. Zalesskiy, E. Danieli, B. Blümich, V. P. Ananikov, *Chem. Rev.* **2014**, *114*, 5641.
[25] J. A. Tang, A. Jerschow, *Magn. Reson. Chem.* **2010**, *48*, 763.
[26] K. Halbach, *Nuclear Instruments and Methods in Physics Research* **1980**, *169*, 1.
[27] K. A. McLean, K. B. McAuley, *The Canadian Journal of Chemical Engineering* **2012**, *90*, 351.
[28] L. Ljung, *System Identification - Theory for the user 2nd edition*, Prentice Hall PTR, Upper Saddle River, NJ **1999**.
[29] T. McKelvey, *Identification of State-Space Models From Time and Frequency Data* (*PhD thesis*, Linköping University, Sweden) **1995**.
[30] C. Ding, H. Peng, *Journal of Bioinformatics and Computational Biology* **2005**, *3*, 185.
[31] R. Isermann, M. Münchhof, *Identification of Dynamic Systems: An Introduction With Applications*, Vol. 85, Springer Berlin, Heidelberg **2011**.
[32] K. E. Häggblom, *IFAC-PapersOnLine* **2016**, *49*, 308.
[33] K. R. Muske, J. B. Rawlings, *AIChE J.* **1993**, *39*, 262.
[34] D. H. Olesen, *Technical University of Denmark* (*M. Sc. thesis,* IMM-M. Sc.-2012–69, Kongens Lyngby, Denmark **2012**.
[35] M. Alhajeri, M. Soroush, *Ind. Eng. Chem. Res.* **2020**, *59*, 4177.

SUPPORTING INFORMATION

Additional supporting information can be found online in the Supporting Information section at the end of this article.

How to cite this article: M. Bornemann-Pfeiffer, K. Meyer, J. Lademann, M. Kraume, M. Maiwald, *Magn Reson Chem* **2023**, 1. https://doi.org/10.1002/mrc.5379